JOURNAL OF GEOPHYSICAL RESEARCH, VOL. 88, NO. A1, PAGES 318-328, JANUARY 1, 1983

QUASI-RELATIVISTIC ELECTRON PRECIPITATION DUE TO INTERACTIONS WITH COHERENT VLF WAVES IN THE MAGNETOSPHERE

H. C. Chang and U. S. Inan

Radioscience Laboratory, Stanford University, Stanford, California 94305

Abstract. The generalized equations of motion for the gyroresonance interaction between energetic electrons and coherent VLF waves in the magnetosphere are employed to study quasi-relativistic electron precipitation. It is suggested that these exact equations be used for particle energies higher than 50 keV (corresponding to a 10% correction in average pitch angle scattering with respect to a nonrelativistic formulation). Based on these equations and the relativistic cyclotron resonance condition, a previous test particle simulation method (Inan, 1977; Inan et al., 1978, 1982) is extended to higher energies and is used to study the wave-particle interactions involving the near-loss-cone quasi-relativistic particles. The root mean square (rms) pitch angle scattering of the near-loss-cone particles and the corresponding precipitated energy spectrum are then calculated and compared. It is argued that the full width at half maximum (FWHM) of the rms scattering pattern would give an upper bound to that of the energy spectrum of the precipitated flux. Furthermore the peak widths are demonstrated to be within the upper limit values measured by recent satellite experiments. This agreement between the computed and measured spectral width lends credence to the suggestions that the observed narrow peaks in precipitated energy spectra may indeed be caused by monochromatic signals injected into the magnetosphere by VLF transmitters.

1. Introduction

It is generally agreed that Doppler-shifted cyclotron resonance interactions between electrons and whistler mode waves in the magnetosphere result in the amplification of the waves, the triggering of discrete emissions, and various wave-particle-wave interactions. During these interactions the electrons are scattered in energy and pitch angle, and their trapped adiabatic motion is perturbed. As a result of such scattering some energetic electrons are precipitated out of the radiation belts and into the atmosphere [Inan et al., 1978]. These precipitated particles can produce secondary ionization, emit X rays, and cause significant perturbation in the lower ionosphere [Rees, 1963; Banks et al., 1974].

For interactions in low L shells, e.g., the inner radiation belt, and for cases when the wave frequency and/or the cold plasma density is low, such gyroresonance interactions involve quasi-relativistic electrons with energies in the range of several tens up to several hundreds of keV. Precipitation of electrons in this energy range in one-to-one correspondence with and therefore believed to be induced by natural VLF/ULF waves (whistlers, chorus emissions, noise bursts) has been reported by numerous authors [Rosenberg et al., 1971; Helliwell et al., 1973; Foster and Rosenberg, 1976; Helliwell et al., 1980; Mende et al., 1980; Rosenberg et al., 1981; Dingle and Carpenter, 1981; Carpenter and LaBelle, 1982].

Recent satellite measurements show that electrons in the drift loss cone precipitate from the slot region between the inner and outer radiation zones (L ~ 2 to ~3.5) and from the outer edge (L ~ 1.5 to ~1.8) of the inner radiation zone [Imhof et al., 1974, 1981a, b; Vampola and Kuck, 1978; Koons et al., 1981]. The energies of the observed precipitating electrons in these experiments are generally in the quasi-relativistic range of 100 to 500 keV. Detailed study of the spectral characteristics of the precipitating electrons has suggested that these electrons were precipitated by first-order cyclotron resonance interactions with nearly monochromatic waves, possibly from ground-based VLF transmitters.

The cyclotron resonance wave-particle interactions have been studied extensively, including the calculation of pitch angle scattering of particles [Roberts, 1966; Inan et al., 1978 and references therein] and the investigation of possible mechanisms for processes of wave growth and damping as well as the triggering of emissions [Dowden, 1962; Brice, 1963; Helliwell and Inan, 1982]. Inan et al. [1978] have performed a detailed study of the nonlinear pitch angle scattering of energetic electrons by coherent longitudinally propagating VLF waves using a test particle approach. In most of these studies the nonrelativistic equations of motion of the particles were used, since most of the work thus far on wave growth and triggering events induced by controlled wave sources involved particles with energies below the quasi-relativistic range [e.g., Helliwell and Katsufrakis, 1974], although the relativistic resonance condition has frequently been used, especially in determining the electron resonance energy from given wave and plasma parameters [e.g. Rosenberg et al., 1971].

Thus, relativistic formulations are necessary in order (1) to more directly compare theoretical and experimental results and (2) to begin to properly assess the effects of man-made VLF waves on the inner radiation belt particle population. From a more general perspective a theoretical formulation of interactions with quasi-relativistic particles and particle precipitation flux resulting from them is important for determining the role of such precipitation in the coupling of the magnetosphere-ionosphere system. Precipitating electrons with energies in the relativistic range are deposited at altitudes of 80-100 km in the ionosphere. There they create ionization enhancements and X rays and can cause major pertur-

Paper number 2A1602.
0148-0227/83/002A-1602$05.00

bations in the D and E regions of the nighttime ionosphere.

In this paper we extend to higher energies the previous test particle simulation of the cyclotron resonance interaction between electrons and coherent VLF waves in the magnetosphere [Inan et al., 1978]. In our formulation, we have not directly included the effects on the wave of the energetic particles and have assumed that the wave field is known in space and time. Justification of this assumption for computing the precipitation flux is given in earlier work [Inan et al., 1978, 1982; Bell and Inan, 1981]. Such effects can be indirectly accounted for by choosing an appropriate wave structure as is done in this paper in connection with Figure 8. Another important assumption in our test particle approach is the fact that we have considered the waves to be propagating longitudinally, presumably in field-aligned ducts of enhanced ionization. Due to the higher magnetic field gradients such ducted guiding of whistler mode waves requires increasingly higher density enhancements at lower L shells. Thus, a more realistic formulation of wave-particle interactions in the inner radiation belt requires consideration of nonducted waves propagating at an angle to the magnetic field.

In the following sections, we first rederive the equations of motion with relativistic effects included. The calculation of precipitation into the loss cone at low L shells is then performed. Finally, the theoretical results are compared with the narrow peaks observed in the energy spectra of electrons precipitating from the inner radiation belt [Imhof et al., 1981a, b].

2. Physics of Relativistic Wave-Particle Interaction

Whistler Mode Wave Structure

Consider a circularly polarized monochromatic whistler mode signal propagating longitudinally along the static magnetic field B_0. In the slowly varying magnetospheric medium the WKB approximation [Budden, 1961] can be used since the variations of medium parameters within the space of one wavelength are negligible. In such a case the wave magnetic field intensity vector can be expressed as

$$\bar{B}_w(z,t) = B_w(z)\left[\bar{a}_x \cos\left(\omega t - \int_0^z k(z)\,dz\right) + \bar{a}_y \sin\left(\omega t - \int_0^z k(z)\,dz\right)\right]$$

where $B_w(z)$ is the magnitude of $\bar{B}_w(z,t)$ and is slowly varying according to the square root of the local refractive index, z is the coordinate along $\bar{B}_0$, ω is the angular wave frequency, k(z) is the wave number, and $\bar{a}_x$ and $\bar{a}_y$ are the unit vectors in the x and y directions, respectively. For whistler mode propagation along the static magnetic field in a cold magnetoplasma, k(z) is given approximately by

$$k(z) = \frac{\omega}{c}\left[1 + \frac{\omega_p(z)^2}{\omega(\omega_H(z) - \omega)}\right]^{1/2}$$

where c is the speed of light, $\omega_p(z)$ is the local electron plasma frequency, and $\omega_H(z)$ is the local electron gyrofrequency.

In the magnetosphere the wave magnetic field intensity changes due to the changing refractive index. Also for ducted wave propagation as is assumed here, the cross-sectional area of the duct varies along the field line, being inversely proportional to the static magnetic field intensity. The intensity of a ducted VLF wave will also vary as the duct cross section changes if the whistler mode wave is assumed to be the superposition of a large number of rays that fill the duct. Including both of these effects, the amplitude $B_w(z)$ of the wave magnetic field can be expressed as

$$B_w(z) = B_{weq}(\omega_H(z)k(z)/\omega_{Heq}k_{eq})^{1/2}$$

where B_{weq}, ω_{Heq}, and k_{eq} are equatorial values. Note that here we have assumed the total power flow of the wave in the duct to be constant. Since B_w, ω_p, ω_H, and k are all slowly varying quantities, in the rest of this paper we drop (z) for the sake of convenience.

Equations of Motion

We now consider the cyclotron resonance interaction between such a coherent wave and relativistic energetic electrons trapped in the flux tube surrounding the field line. This is shown in Figure 1, where $p_\parallel$ and $p_\perp$ represent the parallel and perpendicular components of the particle momentum, respectively. The relation between the total momentum $\bar{p}$ and the total velocity $\bar{v}$ of the particle is given by definition as

$$\bar{p} = m\gamma\bar{v} \tag{1}$$

where m is the rest mass of the particle and $\gamma = 1/\sqrt{1 - v^2/c^2}$, c being the speed of light in vacuum. The kinetic energy of the particle is

$$E = mc^2(\gamma - 1) \tag{2}$$

where mc^2 is the rest energy of the particle, being 511 keV for electrons. Superimposing the adiabatic motion of the particles, defined by $p_\perp^2/B_0$ = constant, on the wave-induced perturbations, the complete equations of motion for the cyclotron resonance wave-particle interaction with relativistic electrons are:

$$\frac{dp_\parallel}{dt} = \frac{eB_w}{m\gamma} p_\perp \sin\phi - \frac{p_\perp^2}{2\omega_H m\gamma}\frac{\partial\omega_H}{\partial z} \tag{3a}$$

$$\frac{dp_\perp}{dt} = -\frac{eB_w}{m\gamma}\left(p_\parallel + \frac{\omega}{k}m\gamma\right)\sin\phi + \frac{p_\perp p_\parallel}{2\omega_H m\gamma}\frac{\partial\omega_H}{\partial z} \tag{3b}$$

$$\frac{d\phi}{dt} = \frac{\omega_H}{\gamma} - \omega - k\frac{p_\parallel}{m\gamma} - \frac{eB_w}{m\gamma}\left(p_\parallel + \frac{\omega}{k}m\gamma\right)\frac{\cos\phi}{p_\perp} \tag{3c}$$

where the coordinate system and the variables are defined in Figure 1, ϕ is the angle between the particle's perpendicular momentum vector $\bar{p}_\perp$ and $(-\bar{B}_w)$, and $\omega_H = eB_0/m$. Equations (3) are written in the laboratory frame. Although (3) describes the particle momentum, the velo-

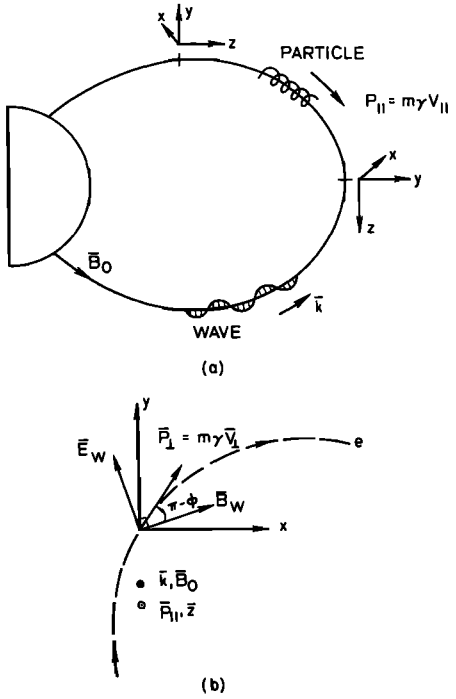

Fig. 1. Coordinate system for the equations of motion. The z axis is everywhere aligned with the magnetic field line. Dashed line indicates the orbit of the electrons in the x-y plane.

city components can be obtained from equation (1) with γ given by

$$\gamma = \sqrt{p^2c^2 + m^2c^4}/mc^2$$

For the nonrelativistic case, $\gamma = 1$, and equations (3) reduce to the nonrelativistic equations of motion which in whole or in part have been used to study VLF wave-particle interactions by many authors [Dysthe, 1971; Bell and Inan, 1981 and references therein].

To the first order, the relativistic formulation can be approximated by a nonrelativistic one with in effect reduction of B_w by a factor γ due to the heavier relativistic mass $m\gamma$. It will be shown in the next section that the scattering of particles and thus the precipitation fluxes are proportional to B_w in the linear regime. Therefore, results obtained from nonrelativistic equations should be corrected to the first order by a factor of γ. For example, nonrelativistic calculation corresponding to particles with energy of 50 keV will require a correction of 10% since $\gamma = 1.1$. Therefore, 50 keV is a reasonable threshold above which the exact equations (3) should be used.

Relativistic Cyclotron Resonance Condition

Since the first terms on the right-hand side in equations (3a) and (3b) are proportional to $\sin\phi$, cumulative changes in $p_{\parallel}$ and $p_{\perp}$ will result only when $\dot{\phi} \simeq 0$. Based on the same arguments as given by Inan et al. [1978], the last term on the right-hand side in equation (3c) is negligible for most magnetospheric parameters unless $v_{\perp} \simeq 0$. Neglecting this term, (3c) can be rewritten as

$$\frac{d}{dt} = k\left[\frac{\omega_H/\gamma - \omega}{k} - v_{\parallel}\right] = k(v_R - v_{\parallel}) \qquad (4)$$

where $v_R = (\omega_H/\gamma - \omega)/k$ is commonly designated as the cyclotron resonance velocity. The relativistic cyclotron resonance condition can thus be written as

$$v_{\parallel} \simeq v_R = (\frac{\omega_H}{\gamma} - \omega)/k \quad \text{or} \quad \omega + kv_{\parallel} \simeq \omega_H/\gamma \qquad (5)$$

Note that $\gamma = (1 - v_{\parallel}^2/c^2\cos^2\alpha)^{-1/2}$, where α is the pitch angle of the resonating particle. Given local values of ω_H and k and a specified value of α, a positive solution for $v_{\parallel}$ can be found:

$$v_{\parallel} \simeq v_R = \frac{-\omega k + [\omega^2k^2 + (\omega_H^2 - \omega^2)(k^2 + \omega_H^2/c^2\cos^2\alpha)]^{1/2}}{k^2 + \omega_H^2/c^2\cos^2\alpha} \qquad (6)$$

It can be shown that for $\mu\cos\alpha > 1$, where μ is the refractive index, the above solution is the only one which satisfies (5). However, for $\mu\cos\alpha < 1$, there exist two solutions: one is positive and is given by (6), the other is negative and corresponds to $\gamma > \omega_H/\omega$. Negative $v_{\parallel}$ represents particles traveling in the same direction as the wave. For typical magnetospheric parameters, $\mu\cos\alpha < 1$ requires a very high pitch angle. For example, for $\mu = 10$, α should at least be 84.3°. In this paper we shall consider only particles with $v_{\parallel}$ as described by (6).

Unlike the nonrelativistic case, the cyclotron resonance parallel velocity for relativistic electrons is a function of pitch angle α. Figure 2 shows the equatorial resonance velocity as a function of α for different values of $\Lambda = \omega/\omega_{Heq}$ for interactions at the geomagnetic equator at

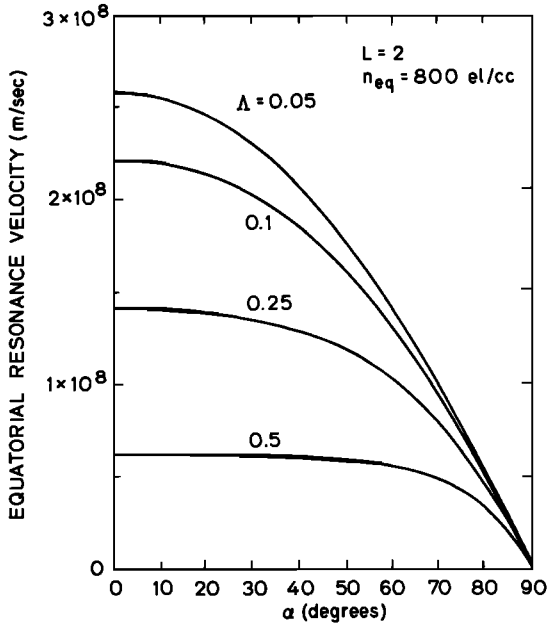

Fig. 2. Equatorial resonance velocity versus equatorial pitch angle for different normalized frequencies $\Lambda = \omega/\omega_{Heq}$. The result shown is for L = 2 and n_{eq} = 800 el/cc.

L = 2, with $f_{Heq} = \omega_{Heq}/2\pi$ = 109.2 kHz, and for cold plasma density of 800 el/cc. The resonance velocity is higher at lower pitch angle and decreases with increasing α. At lower frequencies this decrease is much faster since the total velocity of the particle cannot exceed the speed of light. It is observed from (5) that γ approaches ω_H/ω as $v_\parallel$ approaches zero or α approaches 90°. Therefore, the asymptotic behavior of the resonance velocity near 90° pitch angle is given by

$$v_R \rightarrow c\sqrt{1 - \omega^2/\omega_H^2}\cos\alpha \qquad \alpha \rightarrow 90°$$

Figure 3 shows the energy of the resonant particles as a function of the pitch angle for the corresponding cases in Figure 2. Since γ approaches ω_H/ω, the energy at resonance approaches $mc^2(\omega_H/\omega)$ as α approaches 90°.

For resonant interactions in the inner radiation belt and for cases when the cold plasma density and/or the wave frequency is low, e.g., propagation outside the plasmapause, the energies of the resonant particles are in the quasi-relativistic range. Figure 4 shows the equatorial resonance energy as a function of the equatorial cold plasma density for different frequencies at L = 5 and for α = 3.87°, the half-width of the equatorial loss cone at L = 5. Note for example that for n_{eq} < 20 el/cc, typical of the region outside the plasmapause, waves with frequency less than 700 Hz can interact with particles of energy higher than 100 keV.

Method of Study

Since we shall be considering the wave-induced perturbation of a full distribution of particles, we employ the test particle simulation approach [Inan, 1977; Inan et al., 1978, 1982]. This method basically uses a centered dipole model for the static magnetic field and a diffusive equilibrium model or a collisionless model for the background cold plasma. Subsequently the full equations of motion are integrated for determining the effect of the wave on a sufficient number of test particles that are appropriately distributed in φ, $v_\parallel$, and $v_\perp$. From this the perturbation of the full particle distribution is inferred. For our application we have employed the relativistic equations of motion (3) and the relativistic cyclotron resonance condition (5) and have modified the existing computer model to study the wave-particle interaction involving relativistic particles. Although this model is applicable to relativistic particles of higher energies, in this paper we are particularly interested in the wave-induced perturbation of the quasi-relativistic near-loss-cone particles and their precipitation into the ionosphere. In the next section we study the behavior of these particles during the cyclotron resonance interactions. Subsequently in section 4 we calculate the precipitated fluxes and their energy spectra for selected cases and compare our theoretical results with some recent observations.

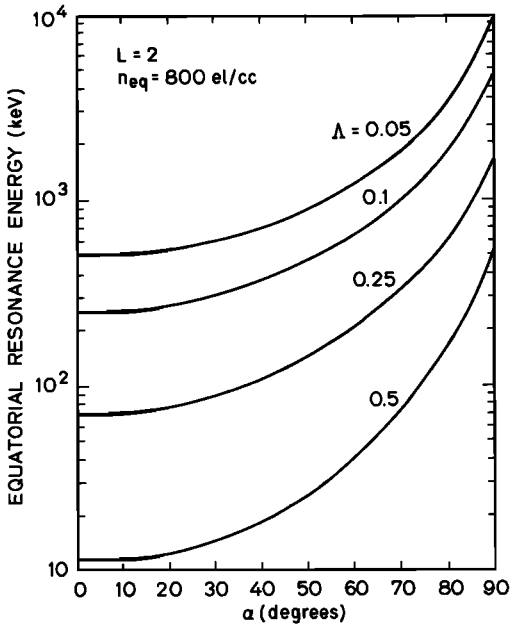

Fig. 3. Equatorial resonance energy versus equatorial pitch angle for the same parameters as in Figure 2.

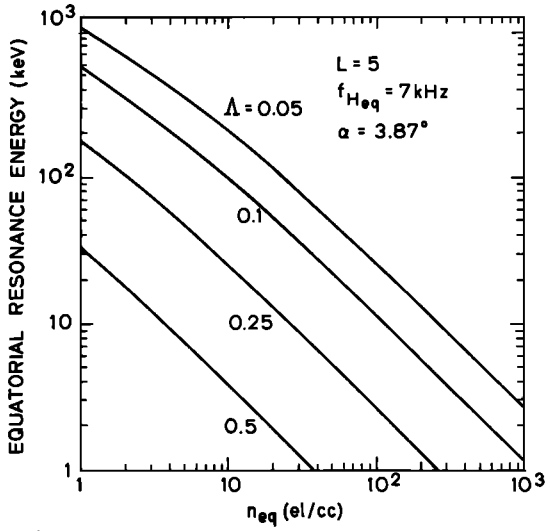

Fig. 4. Equatorial resonance energy versus equatorial cold plasma density for different normalized frequencies Λ. The result shown is for L = 5 with an equatorial gyrofrequency of 7 kHz and a half angle of the equatorial loss cone of 3.87°.

3. Scattering of Near-Loss-Cone Particles

Root Mean Square Scattering

In this section we calculate the efficiency of scattering of the near-loss-cone quasi-relativistic particles by moderate intensity VLF waves. We consider the case of L = 2, representing the outer boundary of the inner radiation belt, and an equatorial cold plasma electron density of 800 el/cc. For a dipole model of the static magnetic field line the equatorial half angle of the loss cone corresponding to a mirror altitude at 100 km is found to be α_{lc} = 16.77°. We consider a monochromatic wave at f = 5.46 kHz (= 0.05 f_{Heq}) with B_w = 7.5 pT at the

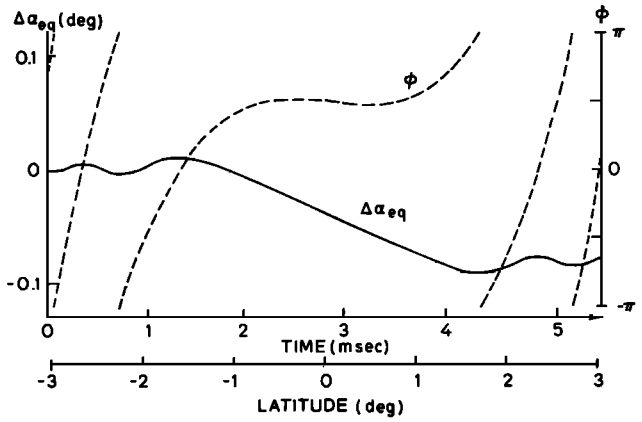

Fig. 5. Trajectory of a relativistic test particle under the influence of a monochromatic wave of 5.46 kHz having B_w = 7.5 pT at L = 2. Both the total scattering $\Delta\alpha_{eq}$ (solid line) and the phase ϕ (dashed lines) are shown as functions of time. The equations of motion are integrated over the time when the particle parallel velocity is within ±2% of the local resonance velocity. The test particle has an energy of 523 keV and an equatorial pitch angle of 16.77°. The initial Larmor phase was taken to be 120°.

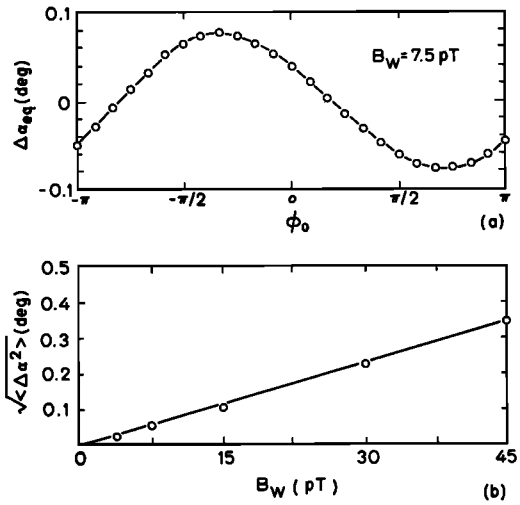

Fig. 6. (a) Total scattering $\Delta\alpha_{eq}$ versus initial phase ϕ_0 for equatorial resonant particles. All other parameters have the same values as in Figure 5. (b) The root mean suqare (rms) scattering as a function of wave intensity for the same resonant particles in Figure 6a.

equator. (This value is selected so that the wave power density would be the same as a wave at f = 0.5 f_{Heq} and with B_w = 5 pT.)

Figure 5 shows the trajectory of an equatorially resonant test particle having an initial Larmor phase (ϕ_0) of 120°, $\alpha = \alpha_{lc}$ = 16.77° and a total energy of 523 keV. The equations of motion are integrated over the time when the particle's parallel velocity is within 2% of the local resonance velocity. For the parameter ranges used in this paper we have found that the wave-induced perturbations can be estimated with at most 10% error when the integration is carried over the time when the particle's parallel velocity is within 2% of the local resonance velocity. Figure 6a shows the total scattering $\Delta\alpha_{eq}$ as a function of ϕ_0 for equatorial resonant particles of the same energy and α. The sinusoidal variation of $\Delta\alpha_{eq}$ with ϕ_0 reveals the linearity of the scattering for the parameters considered, due mainly to the relatively low L shell [Inan, 1977]. This is also demonstrated by Figure 6b which shows the rms scattering of the same particles as a function of wave intensity. It indicates that the rms scattering is proportional to the wave intensity at least up to 45 pT.

Figure 7 shows rms scattering as a function of the particle energy. For each energy we have considered particles uniformly distributed in initial phase and having the same unperturbed pitch angle, i.e., α^0_{eq} = 16.77°. In general, particles with given initial energy higher than 523 keV resonate with the wave in the vicinity of two points on both sides of the equator. The quasi-periodic variation of the scattering is due to the phase coherence between these two resonance points. This phenomenon was described by Ashour-Abdalla [1972] using linear theory. Note that the maximum scattering, which is represented by the peak of the main lobe, occurs when the resonance points are located slightly away from the equator and the strength of scattering decreases rapidly for particles with energy below the equatorial resonance energy. On top of Figure 7 is shown the latitude of resonance as a function of energy. It indicates that the maximum scattering results from interactions within 2° latitude around the equator in this particular case.

The dashed curve in Figure 7 shows the envelope of the rms scattering pattern. This envelope is important since it reveals the relative magnitude of the scattering as a function of the lo-

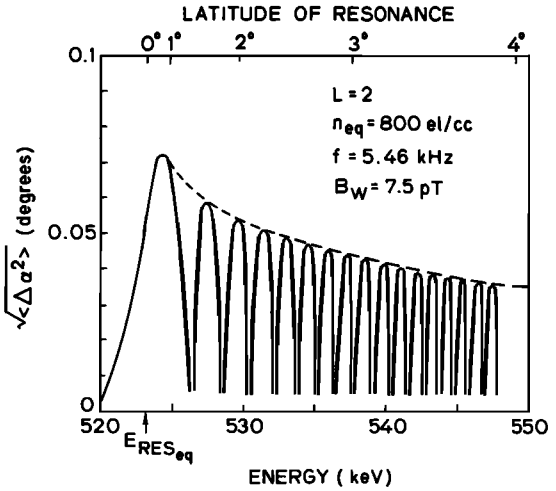

Fig. 7. The rms scattering versus the particle energy for the same magnetoplasma and wave parameters as in Figure 5. For each energy, particles uniformly distributed in initial phase and having the same unperturbed pitch angle α^0_{eq} = 16.77° are considered. The dashed curve shows the envelope of the scattering pattern. Also indicated is the latitude of resonance corresponding to different particle energy.

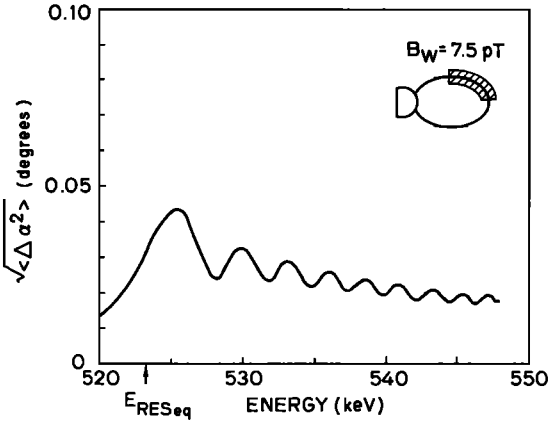

Fig. 8. The rms scattering versus particle energy for a half-sided wave structure. The wave is turned off in the southern part of the field line. All other parameters are the same as in Figure 7.

cation of the resonance point. In the following discussion we use this envelope for the purpose of comparing the wave-induced pitch angle changes for different cases.

Up to now we have considered a wave structure which is distributed on both sides of the equator; the scattering differs if the wave intensity is taken to be zero on the downstream side of the particles. Such a model may represent a wave which has been amplified due to wave-particle interactions near the equator [Helliwell, 1967]. Since this amplification can typically be up to 30 dB [Helliwell and Katsufrakis, 1974], we take the wave intensity to be 7.5 pT on the upstream side of the particles and negligibly small on the other side. Figure 8 shows the rms scattering of the test particles in the same energy range as in Figure 7 due to this half-sided structure. The total pitch angle scattering is less than that of the full wave case since the effective interaction length has been halved. Although the details of the rms scattering patterns for the half-wave and full-wave distributions are different, both patterns show the same dependence on particle energy.

Figure 9 shows the envelope of rms scattering for wave frequencies of 5.46 kHz, 10.9 kHz, and 21.8 kHz corresponding to equatorial resonance energies of 523, 265, and 107 keV, respectively. The wave power density at the equator was taken to be the same for all cases, resulting in different equatorial wave amplitudes, namely, 7.5 pT, 6.4 pT, and 5.6 pT, respectively, due to different refractive indices. For waves at $f = 0.5f_{Heq}$ the amplitude corresponding to this power density would be 5 pT. The result for 5.46 kHz is the same as that shown in Figure 7 and is repeated here for comparison. The initial equatorial pitch angle was taken to be 16.77° in all cases. The peak rms scattering is larger for higher wave frequencies (lower resonance energies) due to the longer interaction times. The dashed curves in Figure 9 show the latitude of resonance as a function of particle energy. For the same percentage deviation above the equatorial resonance energy, the latitude of resonance is further away from the equator for the higher frequency case, resulting in the narrower peak of the rms scattering curve.

The Energy Spectrum of Precipitating Particles

In this section we consider the energy spectrum of the precipitated flux due to interaction of moderate intensity VLF waves with a full distribution (in velocity space) of energetic particles.

Since the typical wave-particle interaction time at L = 2 is short compared to the duration of man-made VLF waves in the magnetosphere (for example, the interaction time for the cases shown in Figure 5 is less than 10 ms), the wave can be considered to be continuous in time. Here we neglect the possible spatial and/or temporal amplification of the wave and assume a wave distribution symmetric around the equator.

The population of the adiabatically trapped energetic particles can be represented by an equatorial distribution function $f(E,\alpha)$, where

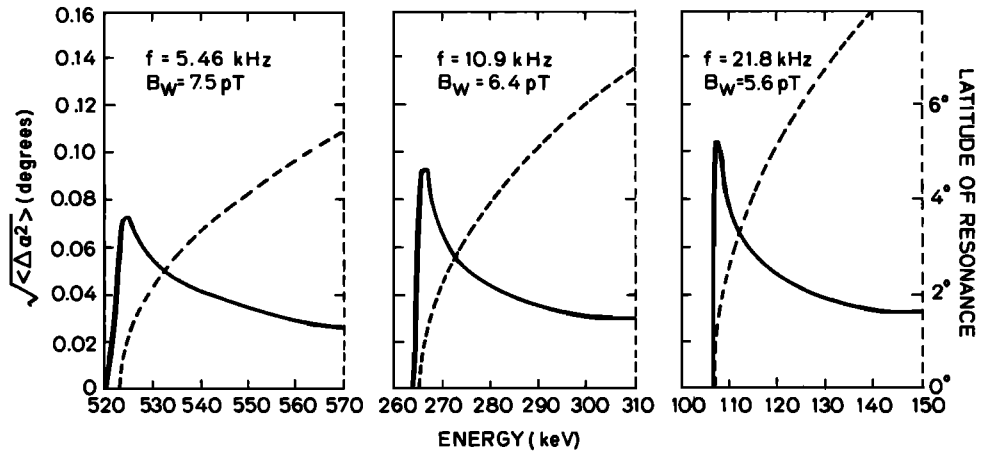

Fig. 9. The envelope of rms scattering pattern versus particle energy for three different wave frequencies at L = 2. The wave power density at the equator has been taken to be the same for all cases, resulting in the slight difference in the equatorial wave amplitude. The f = 5.46 kHz case is identical to the one shown in Figure 7. The dashed curves show the latitude of resonance as a function of particle energy.

E and α are equatorial values. We consider an unperturbed particle distribution of the form

$$f(E,\alpha) = AE^{-n/2}g(\alpha) \qquad \alpha \geq \alpha_{lc}$$
$$f(E,\alpha) = 0 \qquad \alpha < \alpha_{lc} \tag{7}$$

where A is a constant, n/2 is an exponent that can be adjusted to obtain a fit with observed distributions, $g(\alpha)$ represents the pitch angle dependence, and α_{lc} is the angular half width of the loss cone. For the purpose of comparing with observed distributions conventionally described in terms of the differential energy spectrum in el cm^{-2} s^{-1} $ster^{-1}$ keV^{-1}, the constant A can be related to the differential energy spectrum Φ_{E0} of particles at a given energy E_0 (keV) and with $\alpha = 90°$ pitch angle as

$$A = \Phi_{E_0}\left(\frac{m^2}{mc^2}\right)\left(\frac{\gamma_0^5}{\gamma_0^2 - 1}\right) E_0^{n/2} \tag{8}$$

where mc^2 is the rest energy of the electron, m is the rest mass of the electron, and γ_0 is the relativistic factor associated with the energy E_0 (in keV).

The perturbed distribution is obtained by computing the wave-perturbed trajectories of a large number of test particles [Inan et al., 1978]. The precipitated energy flux can then be calculated by integrating the quantity $Evf(E,\alpha)$ over energy and pitch angle within the loss cone of the perturbed distribution, where v is the total velocity of the particle with energy E. To compute the energy spectrum of the flux in el cm^{-2} s^{-1} keV^{-1}, we simply integrate $(1/\Delta E)vf(E,\alpha)$ over the loss cone, where ΔE is the differential energy corresponding to a given energy E. The absolute value of the precipitated flux is proportional to the trapped particle differential energy spectrum Φ_{E0} and the wave intensity B_w adopted for the calculation and therefore can always be scaled up or down according to other given values of Φ_{E0} and B_w as long as B_w is less than B_u, which is defined as the upper limit of the wave intensity below which the linear theory applies [Inan et al., 1978, 1982]. For the parameters considered in this paper, B_u is found to be greater than 50 pT.

Figure 10 shows the calculated energy spectrum of precipitating particles for the case of Figure 7. The energetic particle distribution was taken to be as given by equations (7) or (8), with $g(\alpha) = 1$ (isotropic), $n = 4$ and $\Phi_{E0} = 4.5 \times 10^5$ el cm^{-2} s^{-1} $ster^{-1}$ keV^{-1} for $E_0 = 100$ keV. Note that if we assume the energy dependence of the energetic particle distribution to be E^{-2}, then this gives Φ_E of 10^8 el cm^{-2} s^{-1} $ster^{-1}$ keV^{-1} for 1-keV energy which was the reference flux level used in some of the previous work [Inan et al., 1978, 1982]. For such a trapped distribution and the assumed moderate wave intensity (7.5 pT), the peak value (~10^2 el cm^{-2} s^{-1} keV^{-1}) of the energy spectrum shown in Figure 10 is comparable to those observed data in satellite experiments [Vampola and Kuck, 1978; Imhof et al., 1981a, b].

The energy spectrum of the flux exhibits a phase coherence pattern similar to that of the rms scattering. The small irregularities result from the finite bin width used in the numerical

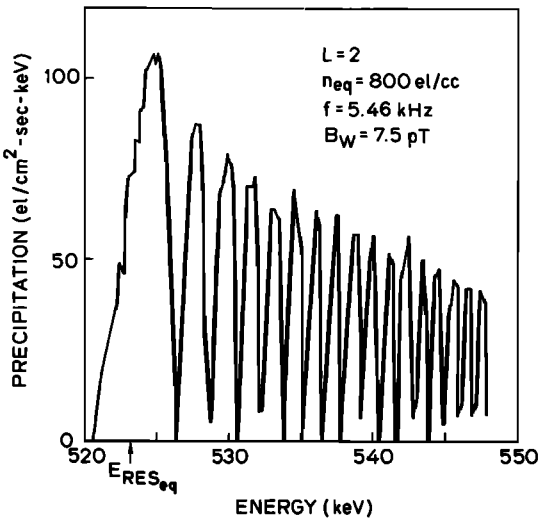

Fig. 10. The energy spectrum of precipitating particles for the case of Figure 7. The energetic particle distribution was taken to be as given by equations (7) and (8), with $g(\alpha) = 1$, $n = 4$, and $\Phi_{E_0} = 4.5 \times 10^5$ el cm^{-2} s^{-1} $ster^{-1}$ keV^{-1} for $E_0 = 100$ keV at 90° pitch angle.

calculations. By comparing Figures 7 and 10 it can be noted that the maxima and minima in the energy spectrum show a one-to-one correspondence to those in the rms scattering pattern with negligible shift in energy. This in turn indicates that the energy change suffered by the particles in negligibly small compared to the pitch angle change since Figure 7 is plotted as a function of initial resonance energy while Figure 10 is in terms of the precipitated or scattered energy. Also note that the rms scattering pattern is not dependent on $f(E,\alpha)$ while the precipitated energy spectrum which results from the integration of $vf(E,\alpha)$ will strongly depend on the assumed distribution function.

The spectral details cannot be detected with presently available particle detectors due to lack of sufficiently high resolution [Imhof et al., 1981a]. However, the envelope of the energy spectrum gives measurable information. The variation of the envelope is determined by the relative strength of scattering given by Figure 7 and the relative population of particles at different energies. The decrease of envelope as energy increases in Figure 10 is faster than that in Figure 7 since we assume an E^{-2} variation of the particle distribution. If we define the equivalent width of the energy spectrum as the full width in energy at half maximum of the flux (FWHM), then the width seen in Figure 10 is ~20 keV. By using the same definition the equivalent width of the rms scattering in Figure 7 is more than 20 keV. The width of the energy spectrum will be further reduced for initial trapped distributions that have steeper falloff in energy.

In the present calculation we have assumed a sharp loss cone edge and an otherwise isotropic initial trapped particle distribution. The maximum pitch angle scattering at a given energy determines the range in pitch angle above the loss cone of the trapped particles which contribute to the precipitation at that energy during a single encounter with the wave. For energies

near the equatorial resonance energy the maximum pitch angle change is larger and thus the contributing range in pitch angle is wider. Due to this factor, particle distributions with a smoother loss cone edge, e.g., a linear or an exponential increase with pitch angle (rather than a step), will result in a narrower width in the precipitated energy spectrum. Assumption of a smoother edge of the loss cone would be more realistic since the particle distributions in the magnetosphere tend to have this property [Lyons and Williams, 1975].

Although the energy spectrum of the precipitated flux is strongly dependent on the assumed trapped particle distribution, the equivalent width of the rms scattering pattern of the near-loss-cone particles can give us an upper bound to the equivalent width of the energy spectrum due to a full distribution of particles. In the next section we compare the experimentally observed peaks in energy spectrum of precipitating particles with the widths predicted by our results.

4. Comparison With Experimental Results

Data for Comparison

Recent satellite experiments have frequently shown that the energy spectra of electrons precipitating from the inner radiation belts contain peaks having central energies which decrease with increasing L value [Vampola and Kuck, 1978; Koons et al., 1981; Imhof et al., 1981a, b]. This observed characteristic suggests that the precipitation may be due to first-order cyclotron resonance interaction of the trapped electrons with monochormatic waves near the magnetic equator. The electrons involved in these interactions had to be precipitated into either the drift loss cone or the local bounce loss cone due to the pitch angle scattering induced by the waves. The observed energies of the precipitating electrons were generally in the range of 100 to 500 keV.

In the following we compare these observed narrow peaks in the precipitated energy spectra with our theoretical predictions. It should be noted that the precipitating electrons which were observed in the drift loss cone might have interacted with the wave near the equatorial region a large number of times during their bounce motions while drifting across a longitude sector. The total pitch angle scattering accumulated from all such individual interactions must thus have been large enough to be observed. We argue here that the spectral content of the precipitating electrons resulting from the cumulative interactions would be similar to that due only to one-pass interaction since the energy changes of these near-loss-cone particles after being pitch angle scattered have been found to be negligibly small compared to their unperturbed energies under conditions of moderate wave intensities. Therefore, the calculations of one-pass scattering of the test particles at the edge of either the drift loss cone or the bounce loss cone will reveal much of the spectral properties of the precipitating electrons.

In the following we choose the data for June 16, 1979, presented by Imhof et al. [1981b] for comparison with our theoretical study. For this day, seven energy spectra at selected L shells from $L \sim 1.57$ to $L \sim 1.75$ were presented. We select three of these spectra, corresponding to $L \sim 1.57$, 1.65, and 1.75, with peak resonance energies of 277, 200, and 120 keV, respectively. It was suggested that a strong monochromatic wave at ~23 kHz measured by plasma wave experiments may have caused the sharp peaks in these spectra [Imhof et al., 1981b]. To derive the equatorial cold plasma densities from the observed peak resonance energies, the waves were assumed to be traveling parallel to the magnetic field lines. For this set of data it was found that the plasma density profile varies as L^{-3}, being consistent with the plasma densities derived from the measured upper hybrid resonance frequencies. From the extrapolated profile the equatorial plasma density corresponding to L = 1.5 on this day is found roughly equal to 4500 el/cc. In our calculation we used this estimated value at L = 1.5 as a reference and assumed an L^{-3} dependence as shown in Figure 11. Also shown in Figure 11 is the value of the equatorial bounce loss cone as a function of L. The loss cone angles are derived from the dipole magnetic field model by taking a mirror height of 100 km. Although propagation is likely to be nonducted in the low-L shell regions, we have assumed ducted longitudinal propagation for purposes of comparison. The equatorial wave amplitudes in all three cases were taken to be 5 pT. This value is within the range of typical intensities of signals from ground-based VLF sources as measured on satellites [Scarabucci, 1969; Inan et al., 1977].

Theoretical Calculations

Having established the magnetospheric parameters for our computations, we present in Figure 12 the computed rms pitch angle scattering versus energy of the near-loss-cone particles induced by one-pass interactions with the 23-kHz waves for the three selected cases. The results are shown in a format similar to that of Figure 9. For cases of lower equatorial resonance energy in Figures 9 and 12 the peak scattering is larger while the absolute width of the peak in keV is narrower. The differences in peak

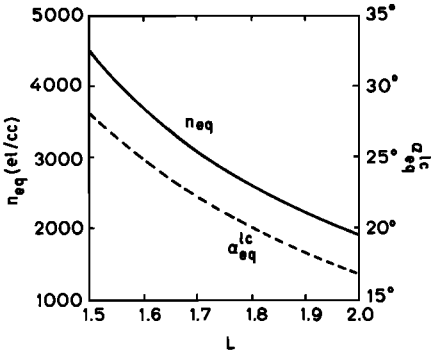

Fig. 11. The equatorial cold plasma density and the equatorial bounce loss cone as functions of L value used for the results shown in Figure 12. The equatorial cold plasma density is proportional to L^{-3}.

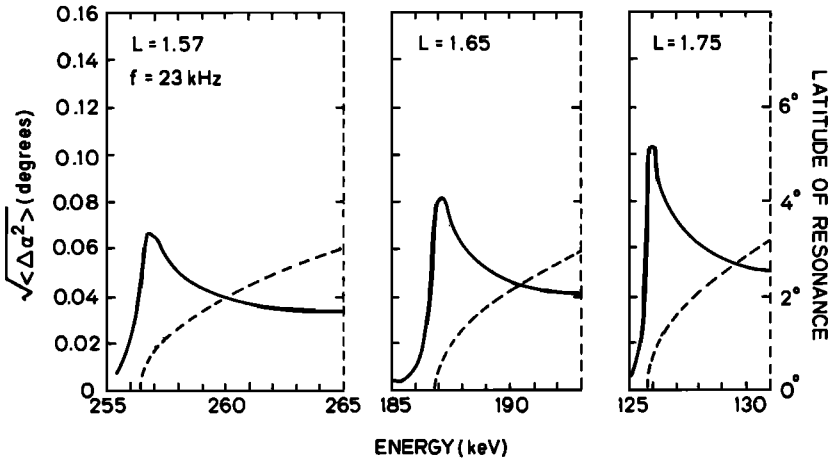

Fig. 12. The envelope of rms scattering pattern versus energy for the near-loss-cone particles resulting from one-pass interactions with a 23-kHz wave on three different L shells. The dashed curves show the latitude of resonance versus energy.

width of the rms scattering for the different cases can be attributed to the same factors as discussed in connection with Figure 9. The peak energies corresponding to L = 1.57, 1.65, and 1.75 cases in Figure 12 are 257, 187, and 126 keV, respectively; these are not exactly equal to those observed by Imhof et al. since the cold plasma densities deduced by them are only approximately equal to the extrapolated densities that we have used. However, this obviously will have negligible effect on our study of the spectral properties.

The rms pitch angle changes in Figure 12 drop to about one half of the maximum value when the latitude of resonance moves ~3° from the equator for all three cases. The resonance energy corresponding to this latitude is less than 10 keV above the equatorial resonance energy in each case. Thus, in terms of our definition of FWHM the peak width is less than 10 keV. For our computations we have assumed a monochromatic wave with equal intensity on both sides of the equator, and the conjugate resonances have been treated as phase-correlated. In the presence of other electromagnetic turbulence, however weak it may be, the dephasing of the two resonances would occur at some latitude above the equator and thus smear out the interference pattern in rms scattering, causing the total scattering to drop to a lower level and thus a possible reduction of the effective peak.

We have shown in the previous section that the peak width in energy of the precipitation flux is generally less than that of the rms scattering. Referring to Figure 12 and the above discussion, the theoretical peak width of the precipitated energy spectra will thus be less than ~10 keV for the cases shown. As reported by Imhof et al. [1981a, b], in some cases the electron energy spectra have FWHM values of the order of 30 keV, which represent upper limit values since they include contributions from the instrument resolution. Widths as narrow as ~20 keV or less could be derived after the instrument resolution is unfolded. Therefore, our theoretical estimation of peak widths is within the possible upper limit values obtained from the experiments. Note that we have assumed a monochromatic wave with a sharply defined wave normal angle at 0°. Therefore the estimated peak results from the dependence of the interaction strength on the latitude of resonance only.

In the following we consider other possible effects which might cause the widening of the observed peaks and thus confirm the presumption that equatorial interactions at these low L shells would produce narrow peaks in the precipitation spectra.

Discussion

While our theoretical results show agreement with those of Imhof et al. [1981a, b], comparison with experimental results is complicated by a number of factors. One is the angular spread of the wave normals in the general case of nonducted propagation.

The parallel resonance velocity expressed by equation (5) is for longitudinally propagating waves. For a first-order correction for oblique propagation with $\bar{k}$ at an angle θ to the static magnetic field, the k in (5) has to be replaced by $k(\theta)\cos\theta$, which is the component of $\bar{k}$ along the magnetic field line, where $k(\theta)$ is the magnitude of $\bar{k}$, a function of θ. Note that k is proportional to the refractive index μ, i.e., $k = (\omega/c)\mu$. For the cases of Figure 12 the equatorial refractive index would increase from 8.30 to 8.48 as L varies from 1.57 to 1.75 under the cold plasma distribution given in Figure 11. If we take the angular spread of wave normals to be within ±30° with respect to the direction of longitudinal propagation, the range of the corresponding equatorial refractive index variation is found to be within ~6% below the equatorial refractive index for the longitudinally propagating wave. The broadening in the equatorial energy bands of electrons effected by this wave normal spread would be approximately 23 keV, 17 keV, and 12 keV for L = 1.57, 1.65, and 1.75, respectively.

One interesting feature revealed by our results is the asymmetry in the rms scattering versus energy curve with respect to the peak. As pointed out in the previous section in connection with Figure 7, the strength of scattering

decreases rapidly for particles with energy below the equatorial resonance energy. If this asymmetry could be detected experimentally, it might be used as an additional test of whether or not the peaks of the precipitated energy spectra are due to wave-particle interactions involving monochromatic waves.

5. Summary and Conclusions

We have rederived the equations of motion for the cyclotron resonance interaction between coherent whistler mode waves and energetic particles with relativistic effects included. A test particle method employing these relativistic equations was then used to study the pitch angle scattering of the near-loss-cone quasi-relativistic electrons trapped in the magnetosphere. The precipitated energy spectrum due to the wave-induced perturbations of a full distribution of particles was also computed. It was found that the FWHM (full width at half maximum) peak width of the rms scattering pattern of the near-loss-cone particles would give an upper bound to the peak width of the associated precipitated energy spectrum under the condition of moderate wave intensities ($B_w \leq 10$ pT) in the low L shell region. We have compared the peak widths in the energy spectra of precipitating electrons observed in recent satellite experiments with our theoretical calculations. It was found that our estimation of peak widths is generally within the upper limit values obtained from the experiments. We have discussed the possible broadening in the spectral peaks resulting from the angular spread of the wave normal.

Our results indicate that, in general, interactions of inner radiation belt particles with monochromatic waves would produce precipitated fluxes with relatively sharp spectral widths, and that therefore the L-dependent narrow peaks observed by low altitude satellite particle detectors could indeed be caused by such interactions.

Acknowledgments. We wish to acknowledge the many valuable discussions we have held with our colleagues at the Radioscience Laboratory. The final manuscript was prepared by K. Faes. This research was supported by the National Aeronautics and Space Administration under contract NGL-05-020-008 and by the National Science Foundation under contract ATM-80-18248. The computer calculations were made on the CDC7600 and CRAY-1 computers of the National Center for Atmospheric Research (NCAR) in Boulder, Colorado. Our use of this facility was made possible by a Computer Resources grant from NCAR.

The Editor thanks B. Edgar and J. C. Siren for their assistance in evaluating this paper.

References

Ashour-Abdalla, M., Amplification of whistler waves in the magnetosphere, Planet. Space Sci., 20, 639, 1972.

Banks, P. M., C. R. Chappell, and A. F. Nagy, A new model for the interaction of auroral electrons with the atmosphere: Spectral degradation, backscatter, optical emission, and ionization, J. Geophys. Res., 79, 1459, 1974.

Bell, T. F., and U. S. Inan, Transient nonlinear pitch angle scattering of energetic electrons by coherent VLF wave packets in the magnetosphere, J. Geophys. Res., 86, 9047, 1981.

Brice, N. M., An explanation of triggered very-low-frequency emissions, J. Geophys. Res., 68, 4626, 1963.

Budden, J. G., Radio Waves in the Ionosphere, Cambridge University Press, New York, 1961.

Carpenter, D. L., and J. W. LaBelle, A study of whistlers correlated with bursts of electron precipitation near L = 2, J. Geophys. Res., 87, 4427, 1982.

Dingle, B., and D. L. Carpenter, Electron precipitation induced by VLF noise bursts at the plasmapause and detected at conjugate ground stations, J. Geophys. Res., 86, 4597, 1981.

Dowden, R. L., Doppler-shifted cyclotron radiation from electrons: A theory of very low frequency emissions from the exosphere, J. Geophys. Res., 67, 1745, 1962.

Dysthe, K. B., Some studeis of triggered whistler emissions, J. Geophys. Res., 76, 6915, 1971.

Foster, J. C., and T. J. Rosenberg, Electron precipitation and VLF emissions associated with cyclotron resonance interactions near the plasmapause, J. Geophys. Res., 81, 2183, 1976.

Helliwell, R. A., A theory of discrete VLF wave emissions from the magnetosphere, J. Geophys. Res., 72, 4773, 1967.

Helliwell, R. A., and U. S. Inan, VLF wave growth and discrete emission triggering in the magnetosphere: A feedback model, J. Geophys. Res., 87, 3537, 1982.

Helliwell, R. A., and J. P. Katsufrakis, VLF wave injection into the magnetosphere from Siple Station, Antarctica, J. Geophys. Res., 79, 2511, 1974.

Helliwell, R. A., J. P. Katsufrakis, and M. L. Trimpi, Whistler-induced amplitude perturbation in VLF propagation, J. Geophys. Res., 78, 4679, 1973.

Helliwell, R. A., S. B. Mende, J. H. Doolittle, W. C. Armstrong, and D. L. Carpenter, Correlations between λ4278 optical emissions and VLF wave events observed at L ~ 4 in the Antarctic, J. Geophys. Res., 85, 3376, 1980.

Imhof, W. L., E. E. Gaines, and J. B. Reagan, Evidence for the resonance precipitation of energetic electrons from the slot region of the radiation belts, J. Geophys. Res., 79, 3141, 1974.

Imhof, W. L., E. E. Gaines, and J. B. Reagan, Observations of multiple, narrow energy peaks in electrons precipitating from the inner radiation belt and their implications for wave-particle interactions, J. Geophys. Res., 86, 1591, 1981a.

Imhof, W. L., R. R. Anderson, J. B. Reagan, and E. E. Gaines, The significance of VLF transmitters in the precipitation of inner belt electrons, J. Geophys. Res., 86, 11,225, 1981b.

Inan, U. S., Non-linear gyroresonant interactions of energetic particles and coherent VLF waves in the magnetosphere, Tech. Rep. 3414-3, Radiosci. Lab., Stanford Electr. Lab., Stanford, Calif., 1977.

Inan, U. S., T. F. Bell, D. L. Carpenter, and R. R. Anderson, Explorer 45 and Imp 6 observations in the magnetosphere of injected waves

from the Siple Station VLF transmitter, J. Geophys. Res., 82, 1177, 1977.
Inan, U. S., T. F. Bell, and R. A. Helliwell, Nonlinear pitch angle scattering of energetic electrons by coherent VLF waves in the magnetosphere, J. Geophys. Res., 83, 3235, 1978.
Inan, U. S., T. F. Bell, and H. C. Chang, Particle precipitation induced by short-duration VLF waves in the magnetosphere, J. Geophys. Res., 87, 6243, 1982.
Koons, H. C., B. C. Edgar, and A. L. Vampola, Precipitation of inner zone electrons by whistler mode waves from VLF transmitters UMS and NWC, J. Geophys. Res., 86, 640, 1981.
Lyons, L. R., and D. J. Williams, The quiet time structure of energetic (35-560 keV) radiation belt electrons, J. Geophys. Res., 80, 943, 1975.
Mende, S. B., R. L. Arnoldy, L. J. Cahill, Jr., J. H. Doolittle, W. C. Armstrong, and A. C. Fraser-Smith, Correlation between λ4278-A optical emissions and a Pc 1 pearl event observed at Siple Station, Antarctica, J. Geophys. Res., 85, 1194, 1980.
Rees, M. H., Auroral ionization and excitation by incident energetic electrons, Planet. Space Sci., 11, 1209, 1963.
Roberts, C. S., Electron loss from the Van Allen zones due to pitch angle scattering by electromagnetic disturbances, in Radiation Trapped in the Earth's Magnetic Field, edited by B. M. McCormac, pp. 403-421, D. Reidel, Hingham, Mass., 1966.
Rosenberg, T. J., R. A. Helliwell, and J. P. Katsufrakis, Electron precipitation associated with discrete very-low-frequency emissions, J. Geophys. Res., 76, 8445, 1971.
Rosenberg, T. J., J. C. Siren, D. L. Matthews, K. Marthinsen, J. A. Holtet, A. Egeland, D. L. Carpenter, and R. A. Helliwell, Conjugacy of electron microbursts and VLF chorus, J. Geophys. Res., 86, 5819, 1981.
Scarabucci, R. L., Interpretation of VLF signals observed on the OGO-4 satellite, Tech. Rep. 3418-2, Radiosci. Lab., Stanford Electr. Lab., Stanford, Calif., 1969.
Vampola, A. L., and G. A. Kuck, Induced precipitation of inner zone electrons, 1. Observations, J. Geophys. Res., 83, 2543, 1978.

(Received August 4, 1982;
revised October 12, 1982;
accepted October 13, 1982.)